ORIGINAL ARTICLE

Second harmonic generation spectroscopy on hybrid plasmonic/dielectric nanoantennas

Heiko Linnenbank[1], Yevgen Grynko[2], Jens Förstner[2] and Stefan Linden[1]

Plasmonic nanoantennas provide unprecedented opportunities to concentrate light fields in subwavelength-sized volumes. By placing a nonlinear dielectric nanoparticle in such a hot spot, one can hope to take advantage of both the field enhancement provided by nanoantennas and the large, nonlinear optical susceptibility of dielectric nanoparticles. To test this concept, we combine gold gap nanoantennas with second-order, nonlinear zinc sulfide nanoparticles, and perform second harmonic generation (SHG) spectroscopy on the combined hybrid dielectric/plasmonic nanoantennas as well as on the individual constituents. We find that SHG from the bare gold nanoantennas, even though it should be forbidden due to symmetry reasons, is several orders of magnitude larger than that of the bare zinc sulfide nanoparticles. Even stronger second harmonic signals are generated by the hybrid dielectric/plasmonic nanoantennas. Control experiments with nanoantennas containing linear lanthanum fluoride nanoparticles reveal; however, that the increased SHG efficiency of the hybrid dielectric/plasmonic nanoantennas does not depend on the nonlinear optical susceptibility of the dielectric nanoparticles but is an effect of the modification of the dielectric environment. The combination of a hybrid dielectric/plasmonic nanoantenna, which is only resonant for the incoming pump light field, with a second nanoantenna, which is resonant for the generated second harmonic light, allows for a further increase in the efficiency of SHG. As the second nanoantenna mediates the coupling of the second harmonic light to the far field, this double-resonant approach also provides us with control over the polarization of the generated light.

INTRODUCTION

Since the pioneering experiments of H. Hertz and G. Marconi, antennas have been essential tools for the manipulation of electromagnetic waves[1,2]. Thus far, antennas have been mainly used for radio and microwave applications, e.g., as components of wireless communication systems or for object detection and ranging[3]. The development of high precision nano-fabrication techniques has additionally revealed promising possibilities for antennas in the optical domain. For instance, one can nowadays fabricate nanometer-sized metallic nanostructures that exhibit resonances in the near infrared and even in the visible spectral regime[4–6]. Like their counterparts in the radio or microwave regime, these so-called plasmonic nanoantennas can be used to funnel-free propagating waves into volumes far smaller than the diffraction limit and vice versa[4–7]. This results in an enormous intensity enhancement for a resonant incoming light field and provides an enhanced far-field coupling for nanoscale light sources.

One class of optical processes with a strong demand for high intensities is the class of nonlinear optical frequency conversion processes[5,8]. The most prominent among them are second harmonic generation (SHG) and parametric down-conversion in noncentrosymmetric bulk crystals (noncentrosymmetry is a necessary condition for electric dipole allowed second-order nonlinear optical processes, see, e.g., Boyd[8], which are both widely used for the generation of high power,

coherent, tunable radiation, from the ultraviolet up to the mid-infrared range[9–11]. Through an increased demand for subwavelength coherent light sources, an interest in subwavelength frequency conversion schemes has also emerged[12–19]. A simple approach could be to directly use nanometer-sized nonlinear dielectric crystals for frequency conversion applications. However, the efficiency of these processes is a superlinear function of the volume of the employed crystals[20]. Therefore, nonlinear frequency conversion processes based on such nonlinear dielectric nanocrystals are intrinsically very weak.

A strategy to overcome the poor conversion efficiency of nonlinear dielectric nanocrystals could be to place the nanocrystals in the hot spots of plasmonic nanoantennas so that one can take advantage of both the plasmonic field-enhancement effect and the large nonlinear optical susceptibility of the dielectric nanoparticles. In several experiments on SHG[21–23] and third harmonic generation (THG)[24,25] from such hybrid plasmonic/dielectric nanoantennas, an enhancement of the nonlinear efficiency of the hybrid dielectric/plasmonic nanoantennas compared to that of the corresponding bare, nonlinear dielectric nanocrystals was indeed observed. These findings apparently support the idea behind the aforementioned strategy, i.e., the increase in the nonlinear signal is caused by a combination of plasmonic field enhancement and a large dielectric nonlinear susceptibility. However, a recent experimental study on THG from gap nanoantennas containing

indium tin oxide (ITO) nanoparticles casts serious doubts on this interpretation[25]. By performing THG spectroscopy on different sized gap nanoantennas, Metzger *et al.* found strong evidence that the nonlinear enhancement of the investigated hybrid plasmonic/dielectric nanoantennas is mainly related to changes in the linear optical properties of the gap nanoantenna resonances due to the presence of the ITO nanoparticles and not the third-order non-linearity of the nanoparticles. Furthermore, they identified the gold nanoantennas as the dominant source of the THG emission.

Plasmonic nanoantennas can be used not only to concentrate the incident pump field in small volumes at the position of the nonlinear nanocrystal but also to help control the coupling of the generated
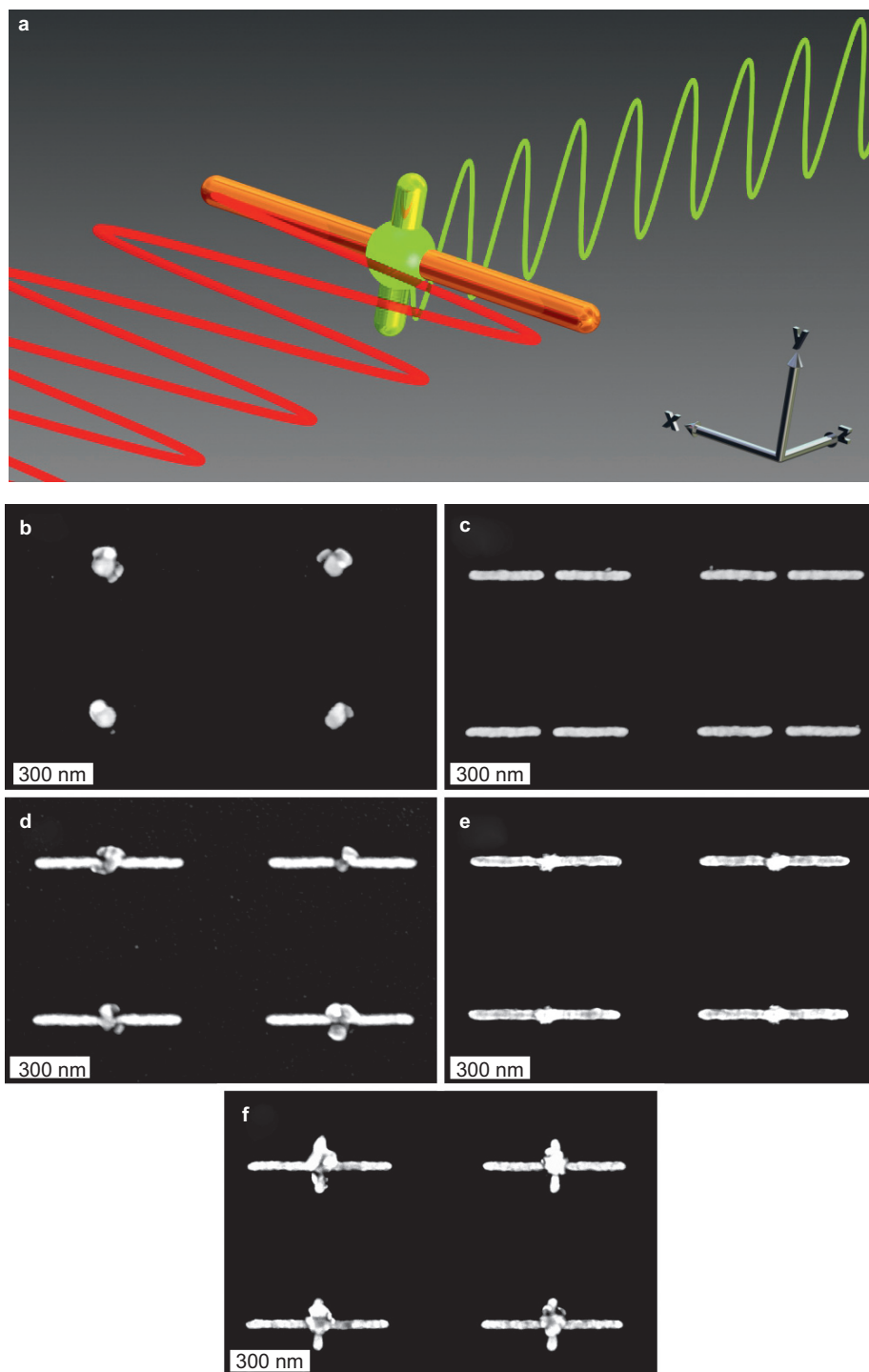

Figure 1 (**a**) Schematic sketch of a double-resonant hybrid plasmonic/dielectric nanoantenna system together with the coordinate system used in this work. (**b**)–(**f**) Top-view SEM micrographs of the investigated ZnS nanostructures, bare gold nanoantennas, nanoantennas with ZnS nanoparticles, nanoantennas with LaF$_3$ nanoparticles, and double-resonant nanoantenna systems with ZnS nanoparticles.

second harmonic (SH) light to the far field. To combine both effects in a single nanostructure, a plasmonic nanoantenna must be designed that it is resonant for both the incoming pump light field and the locally generated SH light field[26–28]. This can, for example, be done by combining two differently sized plasmonic nanoantennas and a nonlinear dielectric nanoparticle to create a double-resonant hybrid plasmonic/dielectric nanoantenna system, as shown in Figure 1a. In a classical resonator picture, this geometry can be seen as a miniaturized version of a double-resonant cavity used for intra-cavity SHG, which is known to show higher conversion efficiencies than the case in which only the pump light or the SH light is resonantly enhanced[29–32].

In this work, we study the origin of the SHG enhancement in hybrid plasmonic/dielectric nanoantennas. For this purpose, we combine gap nanoantennas made of gold either with nonlinear zinc sulfide nano-particles or linear (in this context, linear means that the second-order nonlinear susceptibility vanishes due to symmetry reasons) lan-thanum fluoride nanoparticles and perform linear extinction mea-surements and SHG spectroscopy on the hybrid dielectric/ plasmonic nanoantennas, as well as on the individual constituents. We find that the SHG efficiency of the bare gold nanoantennas is several orders of magnitude higher than that of the zinc sulfide nano-particles. A comparison of the SHG efficiency of the two types of hybrid nanoantennas shows that this process is very sensitive to changes of the environment of the nanoantennas, but independent of the nonlinear properties of the dielectric nanoparticles. Additionally, we combine two plasmonic nanoantennas such that one nanoantenna is resonant for the pump field, while the second nanoantenna is resonant for the generated SH light. With this approach, we can not only achieve a higher conversion efficiency but also control the polarization state of the generated SH light.

MATERIALS AND METHODS

The preparation of the nanoantennas was done by a two-step electron beam lithography process. In the first electron beam lithography step, we fabricated several arrays of gold nanoantennas and additional alignment marks. In the second lithography step, prior to the expo-sure, the positions of those marks were detected to determine the positions of the nanoantennas. Subsequently, the electron beam resist was selectively exposed at the regions of the gaps of the antennas. After development, we deposited a 60-nm thin dielectric layer via high vacuum thermal evaporation and performed a lift-off process. For one sample (sample 1), zinc sulfide (ZnS), which is a wide band gap noncentrosymmetric semiconductor, was used as a dielectric, whereas for a second sample (sample 2), lanthanum fluoride (LaF$_3$), which has a comparable refractive index to ZnS but a centrosymmetric crystal structure, was used instead. For our experiments, we chose a gap nanoantenna design, which is known to exhibit only a weak intrinsic SHG efficiency[33–35]. The nanoantennas had a width and a height of 40 nm, a gap width of 50 nm, and were arranged on a 900 nm × 600 nm lattice with a size of 40 μm × 40 μm. The lengths of the nanoantennas (approximately 300 nm per antenna arm) were chosen such that the linear extinction has a maximum at approximately 1500 nm wave-length. Additionally, dielectric nanoparticles were arranged on a 900 nm × 600 nm lattice without antennas but with a comparable size to those located in the nanoantenna gaps, and thin dielectric films were fabricated in the second lithography step. In Figure 1, SEM micro-graphs of the investigated (b) ZnS nanostructures, (c) bare gold nanoantennas, (d) nanoantennas with ZnS nanoparticles, (e) nanoan-tennas with LaF$_3$ nanoparticles, and (f) double-resonant nanoantenna

systems with ZnS nanoparticles are shown. The SEM micrographs indicate that the ZnS is in a crystalline state.

The linear response of the nanoantenna arrays was measured with polarization selective, normal-incidence, white-light transmission spectroscopy over a wavelength range from 600 nm to 1700 nm. For the SHG spectroscopy measurements, we employed a double-pass optical parametric generator (OPG), delivering pulses with a length of 200–300 fs (spectral full width at half maximum 8–40 nm) at 42 MHz repetition rate, tunable from 1400 nm to 1650 nm, as pump light source[36]. The average power of the pump beam was attenuated to below 10 mW. Above this value, the nonlinear response of the nanoan-tenna arrays would begin to drop with time, indicating an optical-induced thermal damage. The linear polarization in the *x*-direction (see coordinate system in Figure 1a) of the pump beam was controlled by the combination of a polarizer and a half-wave plate. The pump light was focused down to an approximately 30-μm spot diameter under normal incidence (*z*-direction). The SHG signal was recorded in transmission with a charge-coupled device spectrometer for differ-ent pump wavelengths in steps of approximately 10 nm. Additionally, a polarizer could be used to characterize the polarization of the SH light. If not stated otherwise, the SHG signal was recorded polarization unselective. To eliminate any parasitic effects due to changes in the pulse shape and beam divergence when tuning the OPG, the SHG signals from the nanoantenna and nanoparticle arrays were spectrally integrated and referenced to the weak SHG signal obtained from the ITO-covered substrate surface. A dielectric OD 4 longpass filter in front of the focusing lens was used to block any parasitic-generated SH light from the OPG or used optics. Furthermore, to make sure that the recorded SHG signal indeed stemmed from the investigated struc-tures, we recorded after each measurement spectra without any sample and also with a glass substrate without ITO under the same conditions as those used in the actual measurement.

RESULTS AND DISCUSSION

To first assess the nonlinear properties of the thermal evaporated dielectrics, we compared the SHG efficiency of the nanoparticle arrays and thin films made from ZnS and LaF$_3$ with the SHG efficiency of the underlying ITO-covered substrate surface at a fixed wavelength of 1480 nm (see Figure 2). In the case of the LaF$_3$ nanoparticle arrays/ thin films, the SHG efficiency was weaker than that of the underlying
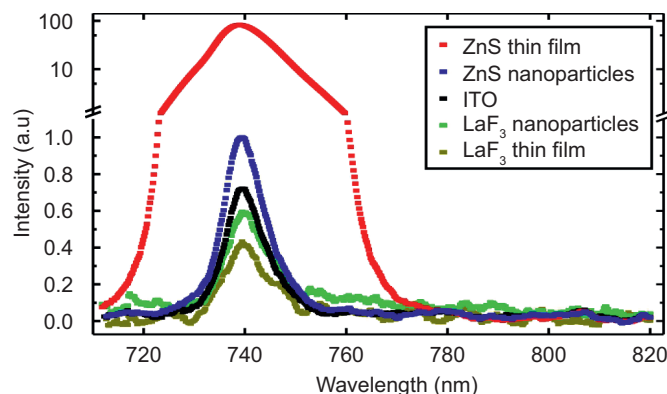
Figure 2 SHG signals obtained, with a fixed pump wavelength of 1480 nm and constant pump intensity, from a thin film of ZnS (red), a ZnS nanoparticle array (blue), a LaF$_3$ nanoparticle array (green), and a thin film of LaF$_3$ (dark yellow). All nanoparticle arrays and thin films were deposited on a glass substrate covered with a thin layer of ITO. The SHG signal from the ITO-covered substrate surface is shown in black.

ITO surface. The most likely reason for this observation is scattering/reflection of the incoming pump light. In the case of the ZnS nanoparticle arrays/thin films, the SHG efficiency was larger by a factor of 1.4/115 than that of the underlying ITO surface. Additionally, the ratio between the SHG efficiency of the ZnS nanoparticle arrays and the thin films is in excellent agreement with the theories for random quasi phase matching, taking their volumes into account[37–40]. Therefore, this preliminary experiment indicates that the ZnS nanoparticles indeed show a second-order nonlinear response, whereas no second-order nonlinear effects can be observed from the LaF$_3$ nanoparticles, as expected.

Next, we compared the SHG efficiency of a nanoantenna array with ZnS nanoparticles with that of an array of bare ZnS nanoparticles (see Figure 1b and 1d) at the center wavelength of the plasmonic resonance of the nanoantennas. Here, we found that the SHG signal of the hybrid plasmonic/dielectric nanoantenna array was larger than that of the ZnS nanoparticle array by a factor of 500 000.

To determine the main source of the nonlinear signal of the hybrid plasmonic/dielectric nanoantennas, we compared the linear and nonlinear spectra of an array of bare gold nanoantennas with that of an array of nanoantennas with ZnS nanoparticles, both located on sample 1. The incorporation of a high refractive index material in the gap of a gold nanoantenna usually leads to a red-shift of the plasmonic resonance[25], which would prevent a direct comparison. To compensate this red-shift, i.e., to obtain congruent plasmonic resonances, we have chosen hybrid nanoantennas, which are approximately 10% shorter than the bare gold nanoantennas, for the comparison. The corresponding extinction (one minus measured transmission) spectra for x-polarized normal incident light are shown as continuous lines in Figure 3a. The connected symbols represent the measured SHG spectra, normalized to the maximum SHG signal of the bare gold nanoantennas. For both antenna arrays, the SHG efficiency closely followed the linear extinction, showing that the SHG was indeed governed by the plasmonic resonance of the nanoantennas. A comparison of the SHG efficiencies of both antenna arrays shows a doubling of the SHG efficiency of the nanoantennas due to the incorporation of the ZnS nanoparticles.

To test whether the increased SHG efficiency really stems from the nonlinear properties of the ZnS, we compared an array of bare gold nanoantennas and a nanoantenna array with LaF$_3$ nanoparticles, both located on sample 2, in the same way as before (see Figure 3b). Here, we again observe a doubling of the SHG efficiency due to the incorporation of a dielectric.

A survey of the presented experimental results allows us to draw several conclusions: (i) Because we obtained the same efficiency enhancement regardless whether we used linear LaF$_3$ or nonlinear ZnS nanoparticles, we conclude that the SHG efficiency enhancement of the plasmonic nanoantennas due to the incorporation of dielectric nanoparticles does not originate from an interplay between the plasmonic field-enhancement effect and the nonlinear optical properties of the dielectric nanoparticle. (ii) The gold nanoantennas are the dominant source of the SH signal, as the LaF$_3$ nanoparticles show no measurable second-order nonlinearity. (iii) The SHG efficiency of plasmonic nanoantennas can be increased by a modification of the dielectric environment. We attribute this effect to a small but measurable narrowing of the resonance line width of the hybrid nanoantennas relative to the bare gold nanoantennas. This is synonymous with an increase of the quality factor Q, which has a strong effect on the nonlinear performance of plasmonic nanostructures[25,41].
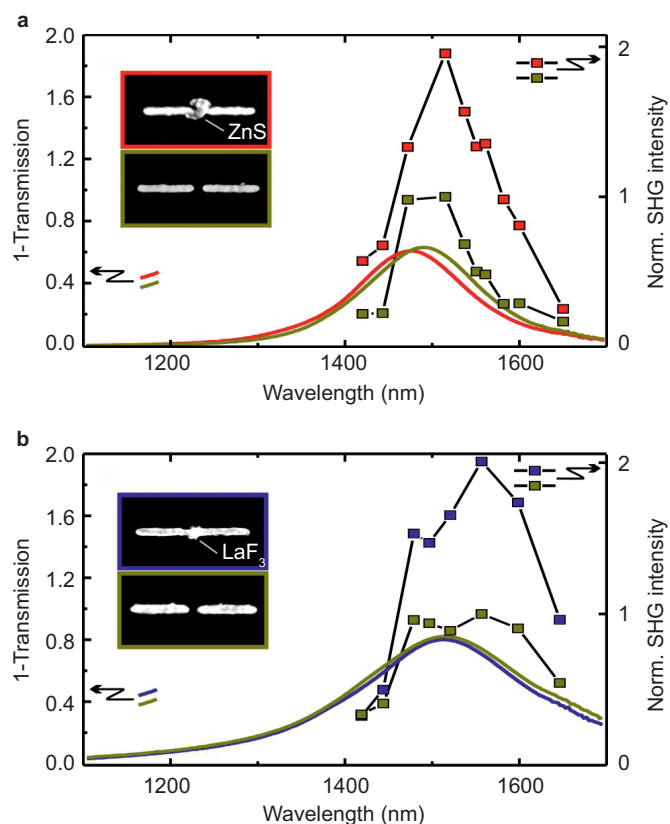

Figure 3 (**a**) Normal-incidence optical extinction (one minus the measured intensity transmission) spectra for x-polarized light (left axis, continuous lines) as well as the SHG intensity (right axis, connected data points) for an array of bare gold nanoantennas (dark yellow) and an array of nanoantennas with ZnS nanoparticles (red), both located on sample 1. (**b**) The same as in (**a**) but for an array of bare gold nanoantennas (dark yellow) and an array of nanoantennas with LaF$_3$ nanoparticles (blue), both located on sample 2. The SHG intensity spectra are both cases normalized to the maxima of the corresponding bare gold nanoantenna arrays.

To quantitatively test this qualitative reasoning and to rule out any experimental artifacts, we have performed numerical calculations using the discontinuous Galerkin time-domain method[42,43] for the bare gold nanoantenna arrays and nanoantenna arrays with a linear dielectric. Our approach self-consistently takes the light propagation at the SH frequency into account and therefore includes SHG reabsorption, emission shaping and the near-to far-field transition. We described the optical response of the metal by the state-of-the-art hydroynamic Maxwell–Vlasov theory[44,45], which takes both surface and bulk contributions into account. Its linear limit corresponds to the Drude free-electron model, for which we have chosen a plasma frequency $\omega_{pl} = 1.33 \times 10^{16}$ rad s^{-1}, a collision frequency $\omega_{col} = 8 \times 10^{13}$ rad s^{-1}, and a background dielectric constant $\varepsilon_\infty = 9.84$. The refractive index of the glass substrate was taken as $n = 1.46$. The geometric parameters of the nanoantennas were adapted from the SEM micrographs shown in Figure 1c and 1d, respectively. The length of the nanoantennas was 350 nm per arm in the case of the bare gold nanoantennas and 325 nm in the case of the hybrid nanoantenna. The width and height were approximately 40 nm. The gap had a width of 60 nm and the size of the dielectric nanoparticles was chosen such that they scarcely touched the nanoantenna arms. The nanoantennas as well as the dielectric nanoparticles were modeled with a surface roughness of approximately 3 nm root mean square by a random

doi:10.1038/lsa.2016.13

displacement of the vertices defining the surfaces of the geometries in the used meshes. This mimicked the experimental conditions and resulted in the observed significant SHG signal. The refractive index of the dielectric nanoparticles was varied to obtain overlapping resonances between the hybrid and bare gold nanoantennas, resulting in a refractive index of $n = 3$. To verify the influence of a change of the dielectric environment of the nanoantennas on their SHG efficiency, the second-order nonlinear coefficient of the dielectric nanoparticles was set equal to zero. The linear extinction calculations, as well as the nonlinear SHG simulations, are presented in Figure 4 in the same way as before the experimental results. Both the enhancement of SHG efficiency and the slight narrowing of the resonance line width of the hybrid nanoantennas relative to the bare gold nanoantennas are nicely reproduced. The slight quantitative deviation between the SHG enhancement in the case of the calculation and the experiment can be attributed to experimental as well as numerical uncertainties. The numerical calculations have been repeated, assuming the dielectric nanoparticle to possess an isotropic second-order susceptibility of 2 pm V^{-1}, which mimics the effective value for a polycrystalline ZnS nanoparticle. The results are identical to those assuming no nonlinearity for the dielectric nanoparticle. Overall, the numerical results strongly support the above qualitative reasoning in that the SHG signal is strongly influenced by a modification of the dielectric environment.

Subsequently, we studied double-resonant nanoantenna systems consisting of two gap nanoantennas-oriented perpendicular to each other (see Figure 1a and 1f). One nanoantenna was designed to be resonant to the pump field (long horizontal-orientated nanoantenna), whereas the other nanoantenna was designed to be resonant to the generated SH light (short vertical-orientated nanoantenna). We performed linear extinction and SHG spectroscopy measurements on an array of double-resonant nanoantenna systems with ZnS nanoparticles. For reference, we used an array of only pump-resonant nanoantennas with ZnS nanoparticles (see Figure 5). Both the pump-resonant nanoantennas and the long nanoantennas of the double-resonant nanoantenna systems had nominally the same length. In the case of the double-resonant nanoantenna systems, we observed a resonance in the extinction spectrum at approximately 780 nm wavelength for *y*-polarized incident light due to the presence of the short nanoantennas, which was absent in the case of the only pump-resonant nanoantennas. The resonance of the long nanoantennas, which was only visible
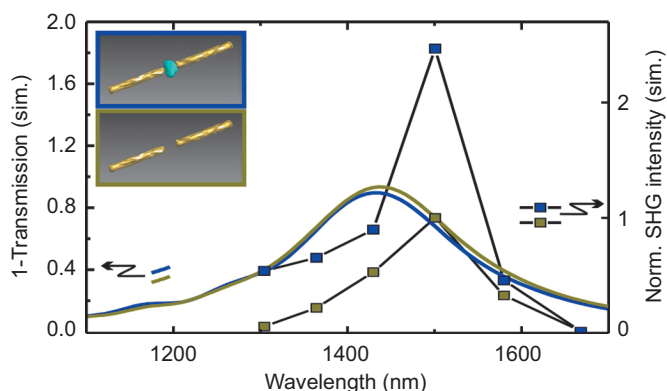
Figure 4 Calculated normal-incidence optical extinction (one minus the calculated intensity transmission) spectra for *x*-polarized light (left axis, continuous lines), as well as the calculated SHG intensity (right axis, connected data points) for an array of bare gold nanoantennas (dark yellow) and an array of nanoantennas with dielectric nanoparticles (blue). The SHG intensity spectra are normalized to the maxima of the corresponding bare gold nanoantenna arrays.
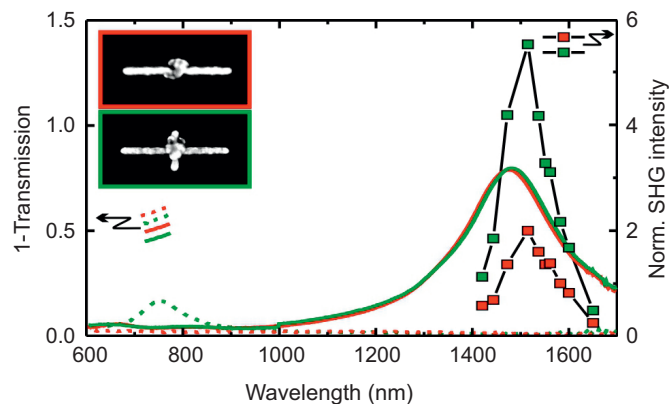
Figure 5 Normal-incidence optical extinction (one minus the measured intensity transmission) spectra for *x*-polarization (left axis, continuous lines) and *y*-polarization (left axis, dashed lines), and the SHG intensity (right axis, connected data points) for an array of ZnS nanoantennas with ZnS nanoparticles (red) and an array of double-resonant nanoantenna systems with ZnS nanoparticles (green). The SHG intensity spectra are both normalized to the maxima of the corresponding bare gold nanoantenna array (see Figure 3a).

for *x*-polarized incident light, was slightly red-shifted, and its line width was marginally increased in the case of the double-resonant systems compared to the only pump-resonant nanoantennas. The red-shift and line width increase originated from a coupling between the short and long nanoantennas. Investigation of the linear extinction spectra of several different double-resonant nanoantenna systems revealed the red-shift and line width increase to be independent of the actual nanoantenna lengths (not shown). By comparing the SHG spectroscopy data of both structures (see Figure 5), we see that the feedback provided by the additional short nanoantennas strongly enhances the SHG efficiency of the hybrid nanoantenna systems, even though the previously mentioned increase of the line width should act counterproductively[25,41].

The additional short nanoantenna in the case of the double-resonant nanoantenna systems does not only enhance the SHG efficiency but also mediates the coupling to the far field of the generated SH light. This becomes evident upon examination of the polarization properties of the SH light generated by the only pump-resonant nanoantennas with ZnS nanoparticles and the double-resonant nanoantenna systems with ZnS nanoparticles. The results are shown in the polar diagrams of Figure 6. In the case of the only pump-resonant nanoantennas, the SH light was weakly polarized along the long nanoantenna axis (*x*-polarized), whereas we observed a significant larger degree of polarization in the case of the double-resonant nanoantenna systems, this time along the axis of the short nanoantennas (*y*-polarized). Our results indicate that double-resonant nanoantenna systems offer the opportunity to influence the far-field properties of the generated SH light.

For the sake of completeness, we checked the SHG efficiency of both nanoantenna geometries for y-polarized pump light. However, in both cases, we could not measure any SHG signal within our measurement resolution.

CONCLUSION

In this work, we compared the SHG efficiency of nonlinear dielectric nanoparticles with plasmonic nanoantennas as well as hybrid dielectric/plasmonic nanoantennas containing either linear or nonlinear dielectric nanoparticles. By combining the results of linear extinction measurements and SHG spectroscopy, we can conclude that an increase of the SHG efficiency of plasmonic nanoantennas obtained
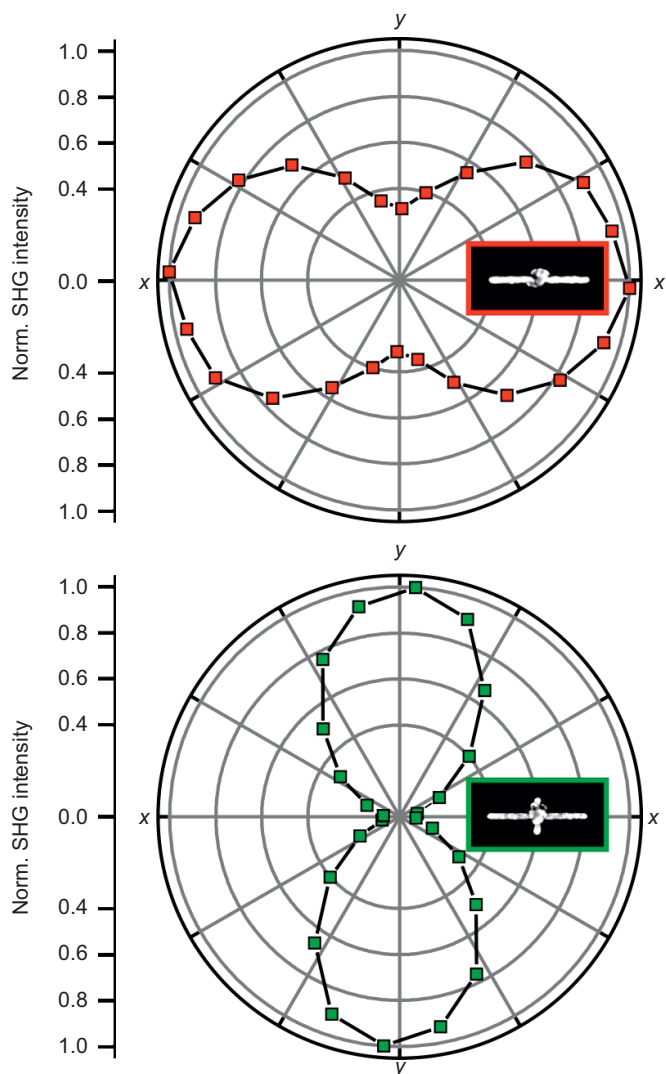
Figure 6 Polar diagrams of the polarization state of the generated SH light from an array of nanoantennas with ZnS nanoparticles (upper diagram) and an array of double-resonant nanoantenna systems with ZnS nanoparticles (lower diagram). In both cases, the pump light was *x*-polarized. All data points are normalized to the maxima of the corresponding data set.

by filling their feed gaps with a dielectric nanoparticle is independent of the nonlinear properties of the dielectric. Furthermore, our experiments showed that the SHG efficiency of plasmonic nanoantennas is several orders of magnitude higher than that of the nonlinear dielectric nanoparticles. The situation might be different if nonlinear dielectrics possessing higher second-order nonlinear coefficients or monocrystalline nonlinear dielectrics with their crystal axis aligned to the local field distributions could be employed.

We additionally showed that a simple combination of two nanoantennas to form a double-resonant nanoantenna system provides not only a strong enhancement of the SHG efficiency but also offers control over the polarization properties of the generated SH signal. In the light of these results, one could also consider the directional emission of the generated SH light mediated by the second nanoantenna. Because the resonances of this system are highly tunable, this design could be easily adapted for a whole variety of frequency conversion processes.

1. Hertz H. Ueber sehr schnelle electrische Schwingungen. *Ann der Phys* 1887; **267**: 421–448.
2. Guglielmo Marconi, Ferdinand Braun. Nobel Lecture: Wireless Telegraphic Communication. http://www.nobelprize.org/nobel_prizes/physics/laureates/1909/marconi-lecture.html, accessed on 10 March 2015.
3. Volakis JL. *Antenna Engineering Handbook*. 4th ed. New York: McGraw-Hill Professional, Access Engineering, 2007.
4. Bharadwaj P, Deutsch B, Novotny L. Optical antennas. *Adv Opt Photon* 2009; **1**: 438–483.
5. Chen PY, Argyropoulos C, Alù A. Enhanced nonlinearities using plasmonic nanoantennas. *Nanophotonics* 2012; **1**: 221–233.
6. Biagioni P, Huang JS, Hecht B. Nanoantennas for visible and infrared radiation. *Rep Prog Phys* 2012; **75**: 024402.
7. Hasan SB, Lederer F, Rockstuhl C. Nonlinear plasmonic antennas. *Mater Today* 2014;17:478–485.
8. Boyd RW. *Nonlinear Optics*. 3rd ed. Burlington, MA: Academic Press, 2008.
9. Fejer MM. Nonlinear optical frequency conversion. *Phys Today* 1994; **47**: 25–32.
10. Petrov V, Ghotbi M, Kokabee O, Esteban-Martin A, Noack F *et al*. Femtosecond nonlinear frequency conversion based on BiB_3O_6. *Laser Photon Rev* 2010; **4**: 53–98.
11. Sowade R, Kießling J, Breunig I. CW laser light tunable from blue to red: OPOs pave the way. *Photonik Int* 2013; **1**: 63–65.
12. Nakayama Y, Pauzauskie PJ, Radenovic A, Onorato RM, Saykally RJ *et al*. Tunable nanowire nonlinear optical probe. *Nature* 2007; **447**: 1098–1101.
13. Zielinski M, Oron D, Chauvat D, Zyss J. Second-harmonic generation from a single core/shell quantum dot. *Small* 2009; **5**: 2835–2840.
14. Vance FW, Lemon BI, Hupp JT. Enormous hyper-Rayleigh scattering from nanocrystalline gold particle suspensions. *J Phys Chem B* 1998; **102**: 10091–10093.
15. Bonacina L, Mugnier Y, Courvoisier F, Le Dantec R, Extermann J *et al*. Polar $Fe(IO_3)_3$ nanocrystals as local probes for nonlinear microscopy. *Appl Phys B* 2007; **87**: 399–403.
16. Hsieh CL, Grange R, Pu Y, Psaltis D. Three-dimensional harmonic holographic microcopy using nanoparticles as probes for cell imaging. *Opt Express* 2009; **17**: 2880–2891.
17. Le Xuan L, Brasselet S, Treussart F, Roch JF, Marquier F *et al*. Balanced homodyne detection of second-harmonic generation from isolated subwavelength emitters. *Appl Phys Lett* 2006; **89**: 121118.
18. Djurišić AB, Leung YH. Optical properties of ZnO nanostructures. *Small* 2006; **2**: 944–961.
19. Danckwerts M, Novotny L. Optical frequency mixing at coupled gold nanoparticles. *Phys Rev Lett* 2007; **98**: 026104.
20. Staedler D, Magouroux T, Hadji R, Joulaud C, Extermann J *et al*. Harmonic nanocrystals for biolabeling: a survey of optical properties and biocompatibility. *ACS Nano* 2012; **6**: 2542–2549.
21. Pu Y, Grange R, Hsieh CL, Psaltis D. Nonlinear optical properties of core-shell nanocavities for enhanced second-harmonic generation. *Phys Rev Lett* 2010; **104**: 207402.
22. Jais PM, von Bilderling C, Bragas AV. Plasmon-enhanced second harmonic generation in semiconductor quantum dots close to metal nanoparticles. *Papers Phys* 2011; **3**: 030002.
23. Grinblat G, Rahmani M, Cortés E, Caldarola M, Comedi D *et al*. High-efficiency second harmonic generation from a single hybrid ZnO nanowire/au plasmonic nano-oligomer. *Nano Lett* 2014; **14**: 6660–6665.
24. Aouani H, Rahmani M, Navarro-Cía M, Maier SA. Third-harmonic-upconversion enhancement from a single semiconductor nanoparticle coupled to a plasmonic antenna. *Nat Nanotechnol* 2014; **9**: 290–294.
25. Metzger B, Hentschel M, Schumacher T, Lippitz M, Ye X *et al*. Doubling the efficiency of third harmonic generation by positioning ITO nanocrystals into the hot-spot of plasmonic gap-antennas. *Nano Lett* 2014; **14**: 2867–2872.
26. Thyagarajan K, Rivier S, Lovera A, Martin OJ. Enhanced second-harmonic generation from double resonant plasmonic antennae. *Opt Express* 2012; **20**: 12860–12865.
27. Harutyunyan H, Volpe G, Quidant R, Novotny L. Enhancing the nonlinear optical response using multifrequency gold-nanowire antennas. *Phys Rev Lett* 2012; **108**: 217403.
28. Chettiar UK, Engheta N. Optical frequency mixing through nanoantenna enhanced difference frequency generation: metatronic mixer. *Phys Rev B* 2012; **86**: 075405.

29 Ashkin A, Boyd GD, Dziedzic JM. Resonant optical second harmonic generation and mixing. *IEEE J Quantum Electron* 1966; **QE 2**: 109–124.

30 Kozlovsky W, Nabors C, Byer R. Efficient second harmonic generation of a diode-laser-pumped CW Nd:YAG laser using monolithic MgO:LiNbO$_3$ external resonant cavities. *IEEE J Quantum Electron* 1988; **24**: 913–919.

31 Zimmermann C, Kallenbach R, Hänsch T, Sandberg J. Doubly-resonant second-harmonic generation in beta-barium-borate. *Opt Comm* 1989; **71**: 229–234.

32 Fiedler K, Schiller S, Paschotta R, Kürz P, Mlynek J. Highly efficient frequency-doubling with a doubly resonant monolithic total-internal-reflection ring-resonator. *Opt Lett* 1993; **18**: 1786–1788.

33 Jin R, Jureller JE, Kim HY, Scherer NF. Correlating second harmonic optical responses of single Ag nanoparticles with morphology. *J Am Chem Soc* 2005; **127**: 12482–12483.

34 Butet J, Duboisset J, Bachelier G, Russier-Antoine I, Benichou E *et al*. Optical second harmonic generation of single metallic nanoparticles embedded in a homogeneous medium. *Nano Lett* 2010; **10**: 1717–1721.

35 Accanto N, Piatkowski L, Renger J, van Hulst NF. Capturing the optical phase response of nanoantennas by coherent second-harmonic microscopy. *Nano Lett* 2014; **14**: 4078–4082.

36 Linnenbank H, Linden S. High repetition rate femtosecond double pass optical parametric generator with more than 2 W tunable output in the NIR. *Opt Express* 2014; **22**: 18072–18077.

37 Baudrier-Raybaut M, Haïdar R, Kupecek P, Lemasson P, Rosencher E. Random quasi-phase-matching in bulk polycrystalline isotropic nonlinear materials. *Nature* 2004; **432**: 374–376.

38 Skipetrov SE. Nonlinear optics: disorder is the new order. *Nature* 2004; **432**: 285–286.

39 Morozov E, Kaminskii A, Chirkin A, Yusupov D. Second optical harmonic generation in nonlinear crystals with a disordered domain structure. *J Exp Theor Phys* 2001; **73**: 647–650.

40 Vidal X, Martorell J. Generation of light in media with a random distribution of nonlinear domains. *Phys Rev Lett* 2006; **97**: 013902.

41 Linden S, Niesler FBP, Förstner J, Grynko Y, Meier T *et al*. Collective effects in second-harmonic generation from split-ring-resonator arrays. *Phys Rev Lett* 2012; **109**: 015502.

42 Hesthaven JS, Warburton T. Nodal Discontinuous Galerkin Methods: Algorithms, Analysis, and Applications. New York: Springer, 2008.

43 Stannigel K, König M, Niegemann J, Busch K. Discontinuous Galerkin time-domain computations of metallic nanostructures. *Opt Express* 2009; **17**:14934–14947.

44 Akhiezer A. *Plasma Electrodynamics: Nonlinear Theory and Fluctuations*, Vol. 2. New York: Pergamon Press, 1975.

45 Zeng Y, Hoyer W, Liu J, Koch SW, Moloney JV. Classical theory for second-harmonic generation from metallic nanoparticles. *Phys Rev B* 2009; **79**: 235109.